Influences of refrigerant-based nanofluid composition and heating condition on the migration of nanoparticles during pool boiling. Part II: Model development and validation

Hao Peng [a,b], Guoliang Ding [a,*], Haitao Hu [a]

[a] Institute of Refrigeration and Cryogenics, Shanghai Jiaotong University, 800 Dongchuan Road, Shanghai 200240, China
[b] Key Laboratory of Microgravity (National Microgravity Laboratory)/CAS, Institute of Mechanics, Chinese Academy of Sciences (CAS), 15 Beisihuan Xilu, Beijing 100190, China

ARTICLE INFO

ABSTRACT

The objective of this study is to propose a model for predicting the migration characteristics of nanoparticles during the refrigerant-based nanofluid pool boiling. In establishing the present model, the departure and rising processes of bubble, as well as the movement of nanoparticles in the liquid-phase are firstly simulated; then the capture of nanoparticles by bubble and the escape of nanoparticles from the liquid—vapor interface are simulated; finally, the migration ratio of nanoparticles is obtained by flotation theory combining the analysis on the boiling process. The proposed model can predict the influences of nanoparticle type, nanoparticle size, refrigerant type, mass fraction of lubricating oil, heat flux and initial liquid-level height on the migration of nanoparticles. The migration ratio of nanoparticles predicted by the model can agree with 90% of the experimental data of within a deviation of $\pm 20\%$, and the mean deviation is 12.1%.

© 2011 Elsevier Ltd and IIR. All rights reserved.

Influences de la composition et le chauffage d'un nanofluide sur la migration des nanoparticules lors de l'ébullition libre. Partie II : développement et validation du modèle

* Corresponding author. Tel.: +86 21 34206378; fax: +86 21 34206814.
  E-mail address: glding@sjtu.edu.cn (G. Ding).

Nomenclature

a	acceleration (m s^{-2})
A	heating surface area (m^2)
C	ratio of mass of nanoparticles in the liquid-phase to the volume of liquid-phase
C_c	Cunningham slip correction factor to Stokes' drag law
C_D	resistance coefficient
C_p	isobaric specific heat (J kg^{-1} K^{-1})
d	diameter of bubble or nanoparticle (m)
D	bottom diameter of vessel (m)
E	nanoparticles capture efficiency
Eo	Eötvös number
f	departure frequency of bubble (s^{-1})
F	force (N)
G	random number with normal distribution
h_{fg}	latent heat of vaporization (J kg^{-1})
H	height of vessel (m)
k_B	Boltzmann constant, 1.381×10^{-23} J K^{-1}
L	liquid-level height (m)
Loc	location (m)
m	mass (kg)
M	molar mass of gas (kg mol^{-1})
n	number of bubbles
N	active nucleation sites density
p	pressure (Pa)
P	nanoparticles escape probability
q	heat flux (W m^{-2})
Re	Reynolds number
R_m	universal gas constant, 8.314 J mol^{-1} K^{-1}
s	displacement (m)
T	temperature (°C)
u	velocity of spouted nanoparticle (m s^{-1})
v	velocity of bubble or nanoparticle (m s^{-1})
V	volume of bubble (m^3)

Greek symbols

ζ	migration ratio of nanoparticles
φ	initial nanoparticle concentration
Δt	time step (s)
θ	projectile angle (°)
λ	gas molecular mean free path (m)
μ	dynamic viscosity (Pa s)
ρ	density (kg m^{-3})
σ	surface tension (N m^{-1})

Subscripts

a	attachment
am	ambient
b	bubble
buo	buoyancy
Brown	Brownian force
c	collision
d	detachment
D	Brownian diffusion
g	gravity
G	gravity settling
I	interception
In	inertial impaction
L	liquid-phase
max	maximum
n	nanoparticle
o	lubricating oil
r	refrigerant
re	fluid resistance
s	spouted
sat	saturation
t	moment of t
total	resultant force
V	vapor-phase
x	in X-axis
y	in Y-axis

Abbreviation

Pre	predicted values

1. Introduction

In order to quantitatively evaluate the boiling heat transfer of refrigerant-based nanofluid in the heat exchangers of refrigeration systems, the nanoparticle concentration in the liquid-phase and vapor-phase during the boiling process should be accurately calculated. The nanoparticle concentration in the liquid-phase and vapor-phase is related to the migration characteristics of nanoparticles from liquid-phase to vapor-phase during the refrigerant-based nanofluid pool boiling. Therefore, a model for predicting the migration characteristics of nanoparticles from liquid-phase to vapor-phase during the refrigerant-based nanofluid pool boiling is needed to be established. From the experimental results presented in Part I of the present study (Peng et al., 2011), it can be seen that the refrigerant-based nanofluid composition (including nanoparticle type, nanoparticle size, refrigerant type and mass

fraction of lubricating oil) and heating condition (including heat flux and initial liquid-level height) have influences on the migration of nanoparticles, so these influence factors should be reflected in the model.

The existing researches on the modeling of heat transfer characteristics of nanofluids are focused on the convective heat transfer (Khanafer et al., 2003; Putra et al., 2003; Maiga et al., 2005; Wen and Ding, 2005; Xuan and Yao, 2005; Buongiorno, 2006; Namburu et al., 2009), and the results showed that the single-phase convective heat transfer characteristics of nanofluids are affected by nanoparticle concentration. Under shear and viscosity gradient conditions, particles may migrate (Leighton and Acrivos, 1987; Phillips et al., 1992; Morris and Brady, 1998; Liu, 1999), which causes the non-uniform particle concentration and then changes the spatial effective thermophysical properties of nanofluid. In order to determine the non-uniformity in nanoparticle

concentration, a theoretical model has been proposed by Ding and Wen (2005) to predict the migration of nanoparticles in the nanofluid flowing through a pipe, and a numerical simulation based on a combined Euler and Lagrange method has been done by Wen et al. (2009) to predict the migration of nanoparticles in a single channel. These researches reveal the two-phase flow nature of nanofluids and their implications to the convective heat transfer of nanofluids. As the physical nature of the pool boiling heat transfer process is different from that of the convective heat transfer process, especially the generation of the bubbles, the models for predicting the migration of nanoparticles during the convective heat transfer of nanofluid can not directly extended to predict the migration of nanoparticles during the pool boiling. Therefore, a model for predicting the migration characteristics of nanoparticles during the pool boiling should be proposed.

Ding et al. (2009) considered that the adhesion between nanoparticles and bubbles is the main mechanism for the migration of nanoparticles from liquid-phase to vapor-phase during the refrigerant-based nanofluid pool boiling, and proposed a model for predicting the migrated mass of nanoparticles based on the energy conversion theory. Ding et al. model can be used to predict the tendency of the migrated mass changed with the original mass of nanoparticles or the original mass of refrigerant, and the verification results showed the good accuracy when predicting the migrated mass for one type of nanoparticle and one type refrigerant at a single heat flux. As Ding et al. model does not consider the influences of refrigerant-based nanofluid composition and heating condition on the bubble dynamic characteristics or nanoparticle–bubble interaction, it shows poor predictability for the experimental data covering different refrigerant-based nanofluid composition and heating condition, and the mean deviation between Ding et al. model predictions and the experimental data can reach 65.3% (Peng et al., 2011). Distinguishing from Ding et al. model, the existing flotation theory considers the particle–bubble interaction, and can accurately describe the adhesion between nanoparticles and bubbles (Edzwald et al., 1990; Nguyen et al., 1998, 2006; Ralston and Dukhin, 1999; Dai et al., 1999; Yoon, 2000). However, the existing flotation theory can not directly used to predict the migration of nanoparticles from liquid-phase to vapor-phase during pool boiling because they are aimed at the conditions without phase change.

The objective of Part II in this study is to establish a numerical model to predict the migrated ratio of nanoparticles from liquid-phase to vapor-phase in the refrigerant-based nanofluid pool boiling, and the model should accurately predict the influences of refrigerant-based nanofluid composition (including nanoparticle type, nanoparticle size, refrigerant type and mass fraction of lubricating oil) and heating condition (including heat flux and initial liquid-level height) on the migration of nanoparticles.

2. Model description

2.1. Research objective and modeling idea

The migration of nanoparticles from liquid-phase to vapor-phase in the refrigerant-based nanofluid pool boiling can be divided to the following four processes: 1) the departure of bubble from the heating surface, as shown in Fig. 1(a); 2) the
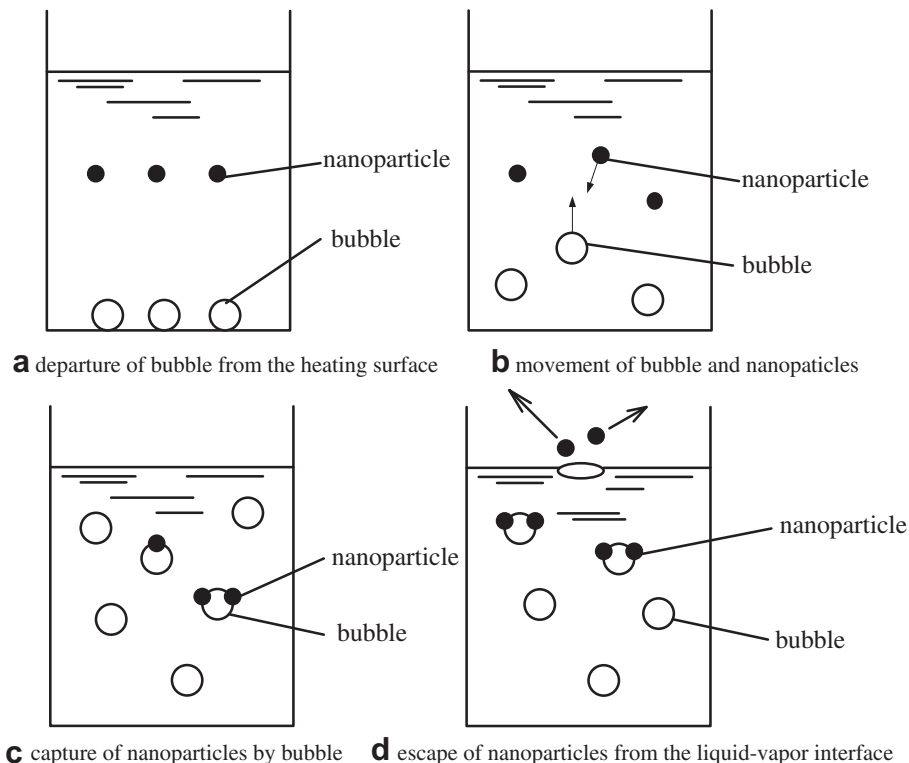

a departure of bubble from the heating surface

b movement of bubble and nanopaticles

c capture of nanoparticles by bubble   **d** escape of nanoparticles from the liquid-vapor interface

Fig. 1 − Schematic of the migration process of nanoparticles from liquid-phase to vapor-phase.

movement of bubble and nanoparticles in the liquid-phase; as shown in Fig. 1(b); 3) the capture of nanoparticles by bubble, as shown in Fig. 1(c); and 4) the escape of nano-particles from the liquid–vapor interface, as shown in Fig. 1(d). In the model to be built in the paper, the above four processes will be described by the four sub-models including the bubble departure sub-model, the bubble and nanoparticle kinetics sub-model, the nanoparticles–bubble interaction sub-model, the nanoparticles escape sub-model, respectively. In order to combine the above four processes and finally output the migration ratio of nanoparticles from the beginning of the pool boiling to a fixed moment, the migration ratio sub-model is also needed. Therefore, the model to

be built in the paper includes five sub-models (i.e., the bubble departure sub-model, the bubble and nanoparticle kinetics sub-model, the nanoparticles–bubble interaction sub-model, the nanoparticles escape sub-model, and the migration ratio sub-model), and the route chart of the model is shown in Fig. 2.

From the above analysis, it can be seen that the interaction between nanoparticles and bubble is the key factor causing the migration of nanoparticles from liquid-phase to vapor-phase. During the pool boiling of refrigerant-based nano-fluid, the mass of nanoparticles in the liquid-phase and the mass of liquid-phase decrease with time, thus the nano-particle concentration in the liquid-phase changes with time,
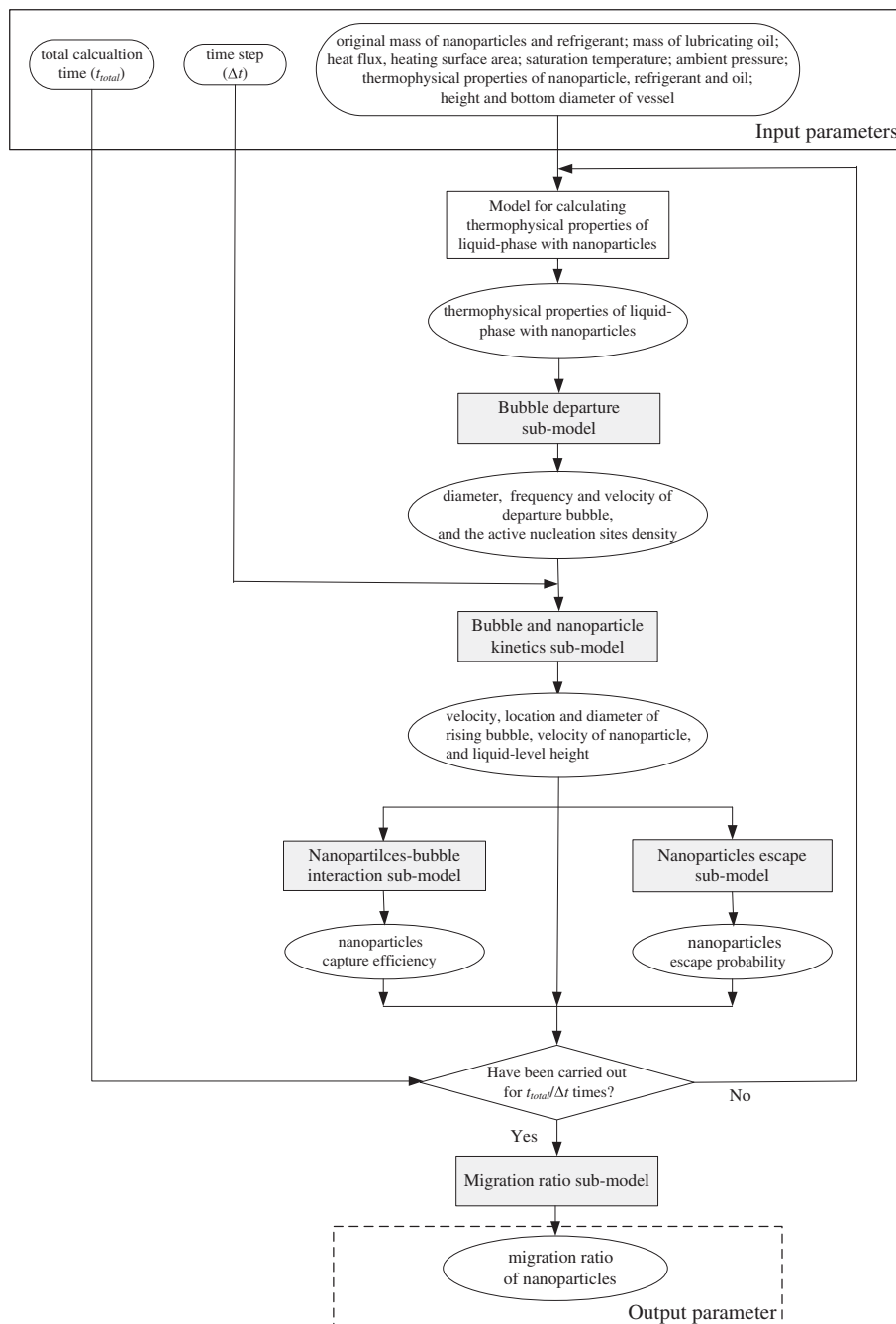

Fig. 2 – The route chart of model.

causing the thermophysical properties of liquid-phase with nanoparticles changes with time, which leads to the bubble dynamics and the migration characteristics of nanoparticles changing with time. In order to reflect the interaction between nanoparticles and bubble, some parameters should be introduced to the model, such as the departure diameter of bubble, the departure frequency of bubble, the velocity of rising bubble, the nanoparticle velocity, the nanoparticles capture efficiency, and the nanoparticles escape probability. In order to reflect the change of migration characteristics of nanoparticles with time, the model should be the dynamic model.

2.2. Bubble departure sub-model

The bubble departure sub-model is used to calculate the departure diameter of bubble, the departure frequency of bubble, the velocity of departure bubble and the active nucleation sites density. In this sub-model, the departure diameter, the departure frequency of bubble and the velocity of departure bubble are calculated by the existing correlations, and the active nucleation sites density are obtained by the energy conservation principle.

The input parameters of the sub-model are $\rho_{L,n}$ (density of liquid-phase with nanoparticles), $C_{p,L,n}$ (isobaric specific heat of liquid-phase with nanoparticles), T_{sat} (saturation temperature), ρ_{b0} (density of departure bubble), h_{fg} (latent heat of vaporization), $\sigma_{L,n}$ (surface tension of liquid-phase with nanoparticles), and q (heat flux). The output parameters of the sub-model are d_{b0} (departure diameter of bubble), f (departure frequency of bubble), v_{b0} (velocity of departure bubble), and N (active nucleation sites density).

The departure diameter of bubble in the pool boiling process can be calculated according to Cole–Rohsenow correlation (Cole and Rosenhow, 1969), as shown in Eq. (1).

$$d_{b0} = 4.65 \times 10^{-4} \left(\frac{\rho_{L,n} C_{p,L,n} T_{sat}}{\rho_{b0} h_{fg}} \right)^{\frac{5}{4}} \left(\frac{\sigma_{L,n}}{g(\rho_{L,n} - \rho_{b0})} \right)^{\frac{1}{2}} \quad (1)$$

The departure frequency of bubble and the velocity of departure bubble and in the pool boiling process can be calculated by Malenkov correlation (Malenkov, 1971), as shown in Eqs. (2) and (3), respectively.

$$f = \frac{1}{\pi d_{b0}} \left\{ \left[\frac{d_{b0} g(\rho_{L,n} - \rho_{b0})}{2(\rho_{L,n} + \rho_{b0})} + \frac{2\sigma_{L,n}(\rho_{L,n} - \rho_{b0})g}{d_{b0} g(\rho_{L,n} + \rho_{b0})} \right]^{1/2} + \frac{q}{h_{fg}\rho_{b0}} \right\} \quad (2)$$

$$v_{b0} = \left[\frac{d_{b0} g(\rho_{L,n} - \rho_{b0})}{2(\rho_{L,n} + \rho_{b0})} + \frac{2\sigma_{L,n}(\rho_{L,n} - \rho_{b0})g}{d_{b0} g(\rho_{L,n} + \rho_{b0})} \right]^{1/2} + \frac{q}{h_{fg}\rho_{b0}} \quad (3)$$

According to the energy conservation principle, the active nucleation sites density can be calculated by Eq. (4).

$$N = \frac{q}{h_{fg}\rho_{b0}\frac{\pi}{6}d_{b0}^3 f} \quad (4)$$

2.3. Bubble and nanoparticle kinetics sub-model

The bubble and nanoparticle kinetics sub-model is used to simulate the movement of bubble and nanoparticle in the liquid-phase, and to calculate the kinetic parameters of bubble and nanoparticle. In the simulation of the movement of bubble,

firstly the forces on bubble are calculated, secondly the velocity and location of rising bubble at different times are calculated by the Newton's second law, and finally the size of rising bubble at different times is calculated according to the pressure balance. In the simulation of the movement of nanoparticle, firstly the forces on nanoparticle in the liquid-phase are calculated, and secondly the velocity of nanoparticle at different times is calculated by the Newton's second law.

The input parameters of the sub-model are ρ_L (density of liquid-phase), $\rho_{L,n}$, ρ_{b0}, ρ_n (density of nanoparticle), d_{b0}, d_n (diameter of nanoparticle), $\sigma_{L,n}$, μ_L (dynamic viscosity of liquid-phase), $\mu_{L,n}$ (dynamic viscosity of liquid-phase with nanoparticles), M (molar mass of gas), T_{sat}, k_B (Boltzmann constant), A (heating surface area), p_0 (ambient pressure above liquid-level), m_{L0} (original mass of liquid-phase), f, v_{b0}, N and Δt (time step). The output parameters of the sub-model are $v_{b,t}$ (velocity of rising bubble at the moment of t), $Loc_{b,t}$ (location of rising bubble at the moment of t), $d_{b,t}$ (diameter of rising bubble at the moment of t), L_t (liquid-level height at the moment of t), $v_{n,t}$ (velocity of nanoparticle at the moment of t).

(1) Forces on bubble

The forces on the bubble include $F_{re,b}$ (fluid resistance force), $F_{buo,b}$ (buoyancy force) and $F_{g,b}$ (gravity force). The resultant force can be calculated as Eq. (5):

$$\vec{F}_{total,b} = \vec{F}_{re,b} + \vec{F}_{buo,b} + \vec{F}_{g,b} \quad (5)$$

In Eq. (5), $F_{buo,b}$ and $F_{g,b}$ are calculated by Eqs. (6) and (7), respectively.

$$F_{buo,b} = \frac{\pi}{6} d_b^3 \rho_{L,n} g \quad (6)$$

$$F_{g,b} = \frac{\pi}{6} d_{b0}^3 \rho_{b0} g \quad (7)$$

$F_{re,b}$ can be calculated by Eq. (8).

$$F_{re,b} = \frac{\pi}{8} d_b^2 \rho_{L,n} C_D v_b^2 \quad (8)$$

In Eq. (8), C_D is the resistance coefficient, and can be calculated by Eq. (9) (Tomiyama et al., 1998).

$$C_D = \max \left[\frac{24}{Re}(1 + 0.15 Re^{0.687}), \frac{8}{3}\frac{Eo}{Eo + 4} \right] \quad (9\text{-}a)$$

$$Re = \frac{\rho_{L,n} v_b d_b}{\mu_{L,n}} \quad (9\text{-}b)$$

$$Eo = \frac{g\rho_{L,n}d_b^2}{\sigma_{L,n}} \quad (9\text{-}c)$$

(2) Velocity and location of rising bubble

The velocity and location of rising bubble are calculated based on the acceleration yielded by Eq. (10):

$$a_b = F_{total,b} \Big/ \left(\frac{\pi}{6} d_{b0}^3 \rho_{b0} \right) \quad (10)$$

The velocity of rising bubble at the moment of t can be calculated as:

$$v_{b,t} = v_{b,t-\Delta t} + \int_0^{\Delta t} a_b dt \quad (11)$$

where, Δt is time step, and $v_{b,t-\Delta t}$ is the velocity before Δt.

The location of rising bubble at the moment of t can be calculated as:

$$Loc_{b,t} = Loc_{b,t-\Delta t} + \int_0^{\Delta t} v_b(t)dt \tag{12}$$

where, $Loc_{b,t-\Delta t}$ is the location before Δt.

(3) Size of rising bubble

In the rising process of bubble, the volume of bubble increases with time because the pressure outside bubble decreases with time. The phenomenon can be described according to the balance between the pressure inside bubble (p_{in}) and the pressure outside bubble (p_{out}), as shown in Eq. (13).

$$\frac{\frac{\pi}{6}d_{b0}^3 \rho_b R_m T_{sat}}{MV_{b,t}} = p_{am} + \rho_{L,n}g(L_t - Loc_{b,t}) + \frac{4\sigma_{L,n}}{d_{b,t}} \tag{13}$$

The left part of Eq. (13) is p_{in}, while the right part of Eq. (13) is p_{out}.

In Eq. (13), $V_{b,t}$ and $d_{b,t}$ are the volume and diameter of bubble at the moment of t; R_m is the universal gas constant, i.e., 8.314 J mol^{-1} K^{-1}; M is the molar mass of gas; p_{am} is the ambient pressure above liquid level (i.e., the vapor-phase pressure); L_t is the liquid-level height at the moment of t.

The relationship between $V_{b,t}$ and $d_{b,t}$ can be expressed as Eq. (14)

$$V_{b,t} = \frac{\pi}{6}d_{b,t}^3 \tag{14}$$

L_t can be calculated by Eq. (15).

$$L_t = \frac{m_{L0} - NfA\left(\frac{\pi}{6}\rho_{b0}d_{b0}^3\right)t}{\rho_L A} \tag{15}$$

According to Eqs. (13)−(15), Eq. (16) can be obtained for calculating $d_{b,t}$

$$\frac{d_{b0}^3 \rho_{b0} R_m T_{sat}}{M d_{b,t}^3} - \frac{4\sigma_{L,n}}{d_{b,t}} = \frac{\rho_{L,n}g}{\rho_L A}\left(m_{L0} - \frac{\pi}{6}NfA\rho_{b0}d_{b0}^3 t - \rho_L A Loc_{b,t}\right) + P_{am} \tag{16}$$

(4) Forces on nanoparticle

The forces on the nanoparticle include $F_{re,n}$ (fluid resistance force), $F_{buo,n}$ (buoyancy force), $F_{g,n}$ (gravity force) and $F_{Brown,n}$ (Brownian force). The resultant force can be calculated as Eq. (17):

$$\vec{F}_{total,n} = \vec{F}_{re,n} + \vec{F}_{buo,n} + \vec{F}_{g,n} + \vec{F}_{Brown,n} \tag{17}$$

In Eq. (17), $F_{buo,n}$, $F_{g,n}$ are calculated by Eqs. (18) and (19), respectively.

$$F_{buo,n} = \frac{\pi}{6}d_n^3 \rho_L g \tag{18}$$

$$F_{g,n} = \frac{\pi}{6}d_n^3 \rho_n g \tag{19}$$

$F_{re,n}$ can calculated by Eq. (20) according to Stokes' drag law.

$$F_{re,n} = 3\pi \mu_L d_n v_n \tag{20}$$

$F_{Brown,n}$ can calculated by the equation proposed by Li and Ahmadi (1992), shown as follows.

$$F_{Brown,n} = G\sqrt{\frac{216\mu_L k_B T_{sat}}{\pi d_n^5 \rho_n^2 \Delta t}} \tag{21}$$

where, G is the random number with normal distribution, the Boltzmann constant $k_B = 1.381 \times 10^{-23}$ J K^{-1}.

(5) Velocity of nanoparticle

The acceleration of nanoparticle is calculated by Eq. (22).

$$a_n = F_{total,n}\Big/\left(\frac{\pi}{6}d_n^3 \rho_n\right) \tag{22}$$

The velocity of nanoparticle at the moment of t can be calculated as:

$$v_{n,t} = v_{n,t-\Delta t} + \int_0^{\Delta t} a_n dt \tag{23}$$

where, Δt is time step, and $v_{n,t-\Delta t}$ is the velocity of nanoparticle before Δt.

2.4. Nanoparticles−bubble interaction sub-model

The nanoparticles−bubble interaction sub-model is used to simulate the capture of nanoparticles by bubble. In this sub-model, the nanoparticles capture efficiency is calculated according to flotation theory combining particles trapping theory.

The input parameters of the sub-model are $d_{b,t}$, d_n, $v_{b,t}$, $\mu_{L,n}$, k_B and T_{sat}. The output parameter of the sub-model is E_t (nanoparticles capture efficiency at the moment of t).

According to flotation theory (Nguyen et al., 1998; Ralston and Dukhin, 1999; Dai et al., 1999), the process of the particles captured by a bubble can be divided into three steps: the particles-bubble collision, the particles-bubble attachment and the particles-bubble detachment. The particles capture efficiency meaning the fraction of particles captured by a bubble, E, can be calculated by Eq. (24).

$$E = E_c E_a(1 - E_d) \tag{24}$$

where, E_c is the collision efficiency, meaning the fraction of particles colliding with a bubble; E_a is the attachment efficiency, meaning the fraction of particles actually attaching to the bubble surface; E_d is the detachment efficiency, meaning the fraction of particles detaching from the bubble surface.

For the particles with very small size, E_a is approximately equal to 1, and E_d is negligible (Yoon, 2000). Therefore, for nanoparticles, the capture efficiency E can be calculated as:

$$E = E_c \tag{25}$$

The process of particles-bubble collision can be considered as a trapping process of particles by bubble, and the collision efficiency E_c can be expressed as Eq. (26) (Edzwald et al., 1990).

$$E_c = E_{c,D} + E_{c,I} + E_{c,G} + E_{c,In} \tag{26}$$

where, $E_{c,D}$, $E_{c,I}$, $E_{c,G}$ and $E_{c,In}$ are the collision efficiencies

caused by Brownian diffusion, interception, gravity settling and inertial impaction, respectively.

The nanoparticle diameter is much less than the bubble diameter in the pool boiling process of refrigerant-based nanofluid, causing the Brownian diffusion is the controlling mechanism of particles-bubble collision (Nguyen et al., 2006), and $E_{c,I}$, $E_{c,G}$ and $E_{c,In}$ are negligible. Therefore, nanoparticles capture efficiency at the moment of t, E_t, is equal to $E_{c,D,t}$, shown as Eq. (27) (Edzwald et al., 1990).

$$E_t = 0.9\left(\frac{k_B T_{sat}}{\mu_{L,n} d_{b,t} d_n v_{b,t}}\right)^{\frac{2}{3}} \tag{27}$$

2.5. Nanoparticles escape sub-model

The nanoparticles escape sub-model is used to simulate the escape of nanoparticles from the liquid–vapor interface. In this sub-model, firstly the forces on the spouted nanoparticle in the vapor phase are calculated; secondly the velocity and location of nanoparticle at different times are calculated by the Newton's second law; finally the nanoparticles escape probability is obtained.

The input parameters of the sub-model are H (height of vessel), D (bottom diameter of vessel), and L_t. The output parameter of the sub-model is P_t (nanoparticles escape probability).

When the bubbles with the captured nanoparticles rise to the liquid–vapor interface, the bubbles break immediately, and the nanoparticles are spouted to the vapor-phase. Some of spouted nanoparticles will leave from the vessel, and are called as the escaped nanoparticles. However, the other spouted nanoparticles will return to the vessel after a period of time. In order to quantitatively describe the escape of nanoparticles from the liquid–vapor interface, nanoparticles escape probability, P_t, is defined in this paper to be the ratio of the number of escaped nanoparticles to that the number of captured nanoparticles by bubbles.
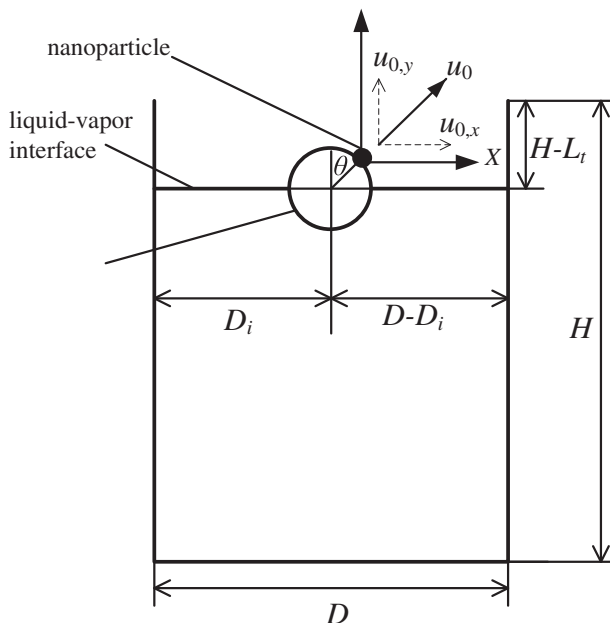

Fig. 3 – Schematic of the spouting process of nanoparticles.

Fig. 3 shows the spouting process of nanoparticles. In Fig. 3, $u_{0,x}$ and $u_{0,y}$ represent the initial velocity in X-axis and Y-axis, respectively. θ is the projectile angle. $u_{0,x}$ and $u_{0,y}$ can be calculated by Eqs. (28) and (29), respectively (Fung and Hamdullahpr, 1993).

$$u_{0,x} = \left(1 - \frac{\theta}{\theta_{max}}\right)u_{0,max}\sin\theta \tag{28}$$

$$u_{0,y} = \left(1 - \frac{\theta}{\theta_{max}}\right)u_{0,max}\cos\theta \tag{29}$$

where, θ_{max} is the maximum projectile angle, and $u_{0,max}$ is the maximum projectile velocity.

The forces on the spouted nanoparticle include $F_{re,n,s}$ (fluid resistance force), $F_{buo,n,s}$ (buoyancy force), $F_{g,n,s}$ (gravity force). The resultant force can be calculated as Eq. (30):

$$\vec{F}_{total,n,s} = \vec{F}_{re,n,s} + \vec{F}_{buo,n,s} + \vec{F}_{g,n,s} \tag{30}$$

In Eq. (30), $F_{buo,n,s}$ and $F_{g,n,s}$ are calculated by Eqs. (31) and (32), respectively.

$$F_{buo,n} = \frac{\pi}{6}d_n^3\rho_V g \tag{31}$$

$$F_{g,n} = \frac{\pi}{6}d_n^3\rho_n g \tag{32}$$

In Eq. (31), ρ_V is the density of vapor-phase.

$F_{re,n,s}$ given by Kleinstreuer (2003) is in the form as follows.

$$F_{re,n,s} = 3\pi\mu_V d_n u/C_c \tag{33}$$

In Eq. (33), C_c is the Cunningham slip correction factor to Stokes' drag law, and can be calculated by Eq. (34).

$$C_c = 1 + \frac{2\lambda}{d_n}(1.257 + 0.4e^{-1.1d_n/\lambda}) \tag{34}$$

where, λ is the gas molecular mean free path (Kleinstreuer, 2003).

As the nanoparticle diameter is very small, the buoyancy force and the gravity force are much less than the fluid resistance force, and can be ignored. Therefore, according to Newton's second law, the velocity at the moment of t in X-axis and Y-axis are calculated by Eqs. (35) and (36), respectively.

$$u_{t,x} = u_{0,x} + \int_0^t \frac{F_{re,n,s,x}}{\frac{\pi}{6}d_n^3\rho_n}dt \tag{35}$$

$$u_{t,y} = u_{0,y} + \int_0^t \frac{F_{re,n,s,y}}{\frac{\pi}{6}d_n^3\rho_n}dt \tag{36}$$

By introducing Eq. (33) to Eqs. (35) and (36), there are:

$$u_{t,x} = u_{0,x}e^{-\frac{18\mu_V t}{\rho_n d_n^2 C_c}} \tag{37}$$

$$u_{t,y} = u_{0,y}e^{-\frac{18\mu_V t}{\rho_n d_n^2 C_c}} \tag{38}$$

According to Eqs. (37) and (38), the displacements at the moment of t in X-axis and Y-axis can be calculated by Eqs. (39) and (40), respectively.

$$s_{t,x} = \frac{\rho_n d_n^2 C_c}{18\mu_V} u_{0,x}\left(1 - e^{-\frac{18\mu_V t}{\rho_n d_n^2 C_c}}\right) \tag{39}$$

$$s_{t,y} = \frac{\rho_n d_n^2 C_c}{18\mu_V} u_{0,y}\left(1 - e^{-\frac{18\mu_V t}{\rho_n d_n^2 C_c}}\right) \tag{40}$$

The nanoparticles spouted in the positive X direction can leave from the vessel if they meet the following condition.

$$\frac{s_{t,x}}{s_{t,y}} \le \frac{D - D_i}{H - L_t} \tag{41}$$

According to Eqs. (28), (29), (39) and (40), Eq. (41) becomes:

$$\theta \le \arctan\left(\frac{D - D_i}{H - L_t}\right) \tag{42}$$

Similarly, the nanoparticles spouted in the negative X direction can leave from the vessel if they meet Eq. (43).

$$\theta \le \arctan\left(\frac{D_i}{H - L_t}\right) \tag{43}$$

Therefore, for the bubble at the location of $(D_i, 0)$, the nanoparticles escape probability, $P(D_i)$, can be calculated by Eq. (44).

$$P(D_i) = \frac{\arctan\left(\frac{D_i}{H - L_t}\right) + \arctan\left(\frac{D - D_i}{H - L_t}\right)}{2\pi} \tag{44}$$

The nanoparticles escape probability for the whole liquid–vapor interface can be considered as the mean value of nanoparticles escape probability for all bubbles at the liquid–vapor interface, and can be calculated as follows.

$$P_t = \frac{\int_0^D P(D_i)dS}{D} = \frac{1}{\pi}\arctan\left(\frac{D}{H - L_t}\right) - \frac{H - L_t}{2\pi D}Ln\left[1 + \frac{D^2}{(H - L_t)^2}\right] \tag{45}$$

2.6.   Migration ratio sub-model

The migration ratio sub-model is used to calculate the migration ratio of nanoparticles from the beginning of the pool boiling to a fixed moment. In this sub-model, the migration ratio of nanoparticles is obtained by flotation theory combining the analysis on the boiling process, and is the output parameter of the whole model.

The input parameters of the sub-model are ρ_L, ρ_{b0}, d_{b0}, m_{L0}, N, f, A, $d_{b,t}$, d_n, $v_{b,t}$, $v_{n,t}$, E_t, P_t, m_{n0} (original mass of nanoparticles), and Δt. The output parameter of the sub-model is $\xi_{t_0-t_j}$ (migration ratio of nanoparticles from the beginning of the pool boiling t_0 to the moment of t_j).

According to flotation theory (Nguyen et al., 1998), the mass of nanoparticles in the liquid-phase changed with time can be expressed as:

$$-\frac{m_{n,t+\Delta t} - m_{n,t}}{\Delta t} = \frac{\pi}{4}(d_{b,t} + d_n)^2(v_{b,t} + v_{n,t})C_t n_b(\Delta t)E_t \tag{46}$$

where, $m_{n,t+\Delta t}$ and $m_{n,t}$ are the mass of nanoparticles in the liquid-phase at the moment of $t + \Delta t$ and t, respectively; C_t is the ratio of mass of nanoparticles in the liquid-phase to the volume of liquid-phase at the moment of t; $n_b(\Delta t)$ is the number of bubbles generated during the time of Δt. C_t and $n_b(\Delta t)$ can be calculated by Eqs. (47) and (48), respectively.

$$C_t = \frac{m_{n,t}\rho_L}{m_{L,0} - NfA\left(\frac{\pi}{6}\rho_{b0}d_{b0}^3\right)t} \tag{47}$$

$$n_b(\Delta t) = NfA\Delta t \tag{48}$$

The nanoparticles escape from liquid-phase to vapor-phase when the bubbles rise to the liquid–vapor interface. Therefore, the migration of nanoparticles only occurs at the moment of t_i, and t_i should meet the following condition.

$$Loc_{b,t_i} = L_{t_i} \tag{49}$$

From the beginning of the pool boiling t_0 to the moment of t_j, the migration ratio of nanoparticles can be calculated by Eq. (50).

$$\xi_{t_0-t_j} = \frac{1}{m_{n0}}\sum_{i=0}^{j-1}\Delta m_{n,t_i-t_{i+1}}P_{t_{i+1}} \tag{50}$$

3.   Algorithm

The algorithm of the model is introduced in detail as follow.

Step 1: Input parameters including m_{n0}, m_{r0}, m_o, d_n, ρ_n, $C_{p,n}$, ρ_r, μ_r, σ_r, $C_{p,r}$, ρ_o, μ_o, σ_o, $C_{p,o}$, h_{fg}, ρ_{b0}, A, D, H, p_{am}, T_{sat}, q, Δt and t_{total}.

Step 2: Calculate the thermophysical properties of liquid-phase with nanoparticles including $C_{p,L,n}$, $\mu_{L,n}$, $\sigma_{L,n}$, and $\rho_{L,n}$ using the equations in Appendix I.

Step 3: Calculate the departure diameter of bubble, the departure frequency of bubble, the velocity of departure bubble and the active nucleation sites density. d_{b0} is calculated by Eq. (1), f is calculated by Eq. (2), v_{b0} is calculated by Eq. (3), and N is calculated by Eq. (4).

Step 4: Simulate the movement of bubble and nanoparticles in the liquid-phase. The forces on the bubble are calculated by Eqs. (5)–(8). $v_{b,t}$, $Loc_{b,t}$, L_t, $d_{b,t}$ are calculated by Eqs. (11), (12), (15) and (16), respectively. The forces on the nanoparticle are calculated by Eqs. (17)–(21), and $v_{n,t}$ is calculated by Eq. (23).

Step 5: Simulate the capture of nanoparticles by bubble. E_t is calculated by Eq. (27).

Step 6: Simulate the escape of nanoparticles from the liquid–vapor interface. P_t is calculated by Eq. (45).

Step 7: Calculate the mass of nanoparticles in the liquid-phase at the moment of t ($m_{n,t}$) by Eqs. (46)–(48).

Step 8: Compare $Loc_{b,t}$ with L_t. If $|Loc_{b,t} - L_t| \leq \varepsilon$, let $t_i = t$. If $Loc_{b,t} < L_t$, let $t = t + \Delta t$, and return to Step 2. If $Loc_{b,t} > L_t$, turn to Step 9.

Step 9: Let $t = (1/2)(t + t - \Delta t)$, and return to Step 2 until $|Loc_{b,t} - L_t| \leq \varepsilon$.

Step 10: Judge the loop. If Steps 2–9 have been carried out for $t_{total}/\Delta t$ times, Step 11 is executed. If not, Step 2 is executed

Step 11: Calculate and output $\xi_{t_0 - t_j}$.

In order to show the present model clearly, the equations used in the simulation are listed in Appendix II.

4.   Experimental validation

The experimental data of the migration ratio of nanoparticles from the beginning to the end of pool boiling in the Part I of the present study are used to validate the model.

In the input parameters to the model, the values of A, D, H, and p_{am} are the same as those used in the experiments in the Part I of the present study, and are 50 mm, 19.6 cm^2, 95 mm, 101.3 kPa. T_{sat} are 47.6 °C, 32.1 °C and 36.1 °C when the host refrigerants are R113, R141b and n-pentane, respectively. The thermophysical properties of nanoparticle and refrigerant are listed in Tables 1 and 2 in the Part I of the present study. The thermophysical properties of lubricating oil RB68EP are referred to the literature (Hu et al., 2008).

Fig. 4 shows the comparison between the predicted values of the model with the experimental data for different nanoparticle types. It can be seen that both the migration ratio of nanoparticles predicted by the model and the experimental data are in the order of Al (20 nm) > Al$_2$O$_3$ (20 nm) > Cu (20 nm. This phenomenon is resulted from the effect of nanoparticle density on the nanoparticle velocity, and this effect can be predicted by the bubble and nanoparticle kinetics sub-model. It can also be seen that the predicted values of the model can agree with 86% of the experimental data within a deviation of −10%−+20%, and the mean deviation is 10.3%.

Fig. 5 shows the comparison between the predicted values of the model with the experimental data for different nanoparticle sizes. It can be seen that both the migration ratio of nanoparticles predicted by the model and the experimental data are in the order of Cu (20 nm) > Cu (50 nm) > Cu (80 nm). This phenomenon is resulted from the effects of nanoparticle size on the nanoparticle velocity as well as the nanoparticles capture efficiency, and these effects can be predicted by the bubble and nanoparticle kinetics sub-model as well as the nanoparticles–bubble interaction sub-model. It can also be seen that the predicted values of the model can agree with 95% of the experimental data within a deviation of ±20%, and the mean deviation is 11.2%.

Fig. 6 shows the comparison between the predicted values of the model with the experimental data for different refrigerant types. It can be seen that that both the migration ratio of nanoparticles predicted by the model and the experimental data are in the order of R141b > R113 > n-pentane. This phenomenon is resulted from the effects of refrigerant dynamic viscosity and refrigerant liquid-phase density on the nanoparticle velocity, the nanoparticles capture efficiency and
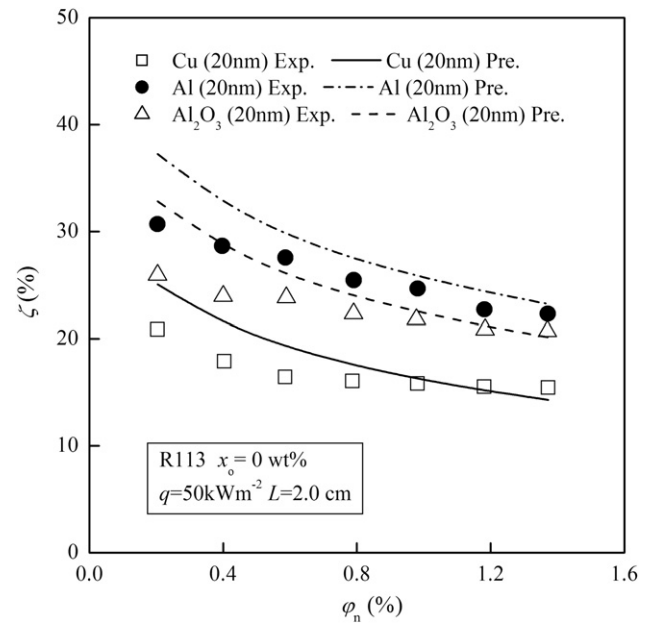

Fig. 4 – Comparison between the predicted values of the model with the experimental data for different nanoparticle types.

the number of bubbles. These effects can be predicted by the bubble and nanoparticle kinetics sub-model, the nanoparticles–bubble interaction sub-model, and the migration ratio sub-model. It can also be seen that the predicted values of the model can agree with 95% of the experimental data within a deviation of −15%−+20%, and the mean deviation is 12.1%.

Fig. 7 shows the comparison between the predicted values of the model with the experimental data for different mass fractions of lubricating oil. It can be seen that both the migration
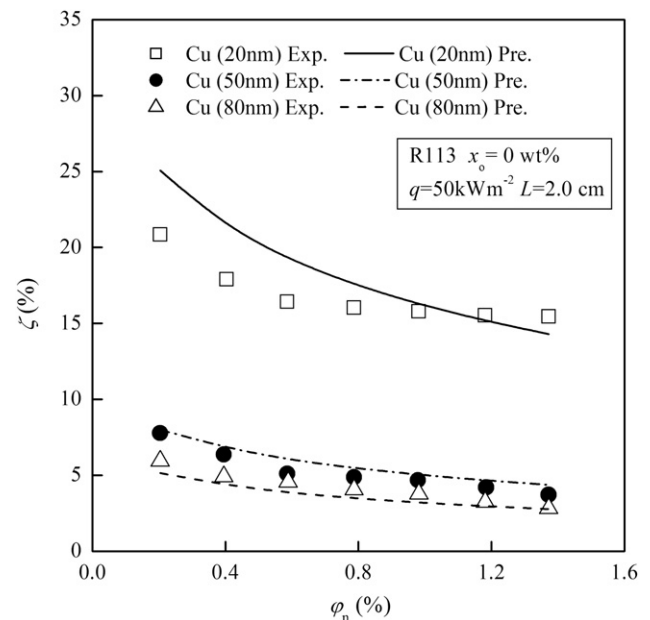

Fig. 5 – Comparison between the predicted values of the model with the experimental data for different nanoparticle sizes.
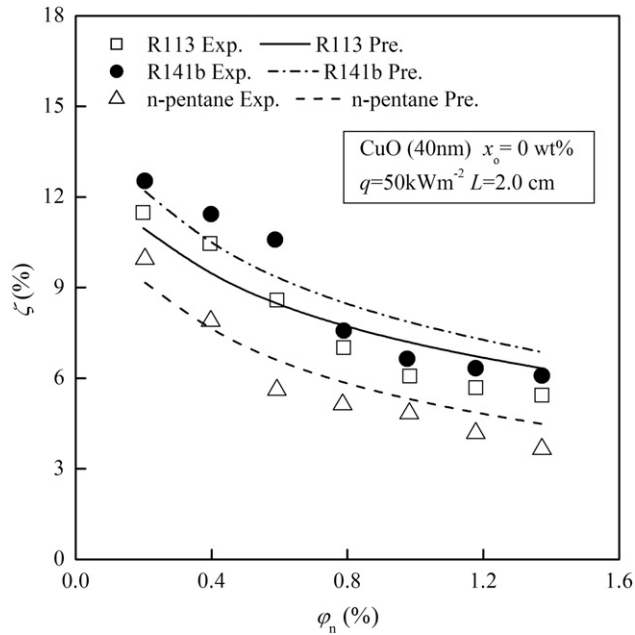
Fig. 6 — Comparison between the predicted values of the model with the experimental data for different refrigerant types.

Fig. 8 — Comparison between the predicted values of the model with the experimental data for different heat fluxes.

ratio of nanoparticles predicted by the model and the experimental data decrease with the increase of mass fraction of lubricating oil. This phenomenon is resulted from the effects of mass fraction of lubricating oil on the bubble departure diameter as well as the nanoparticles capture efficiency, and these effects can be predicted by the bubble departure sub-model as well as the nanoparticles—bubble interaction sub-model. It can also be seen that the predicted values of the model can agree
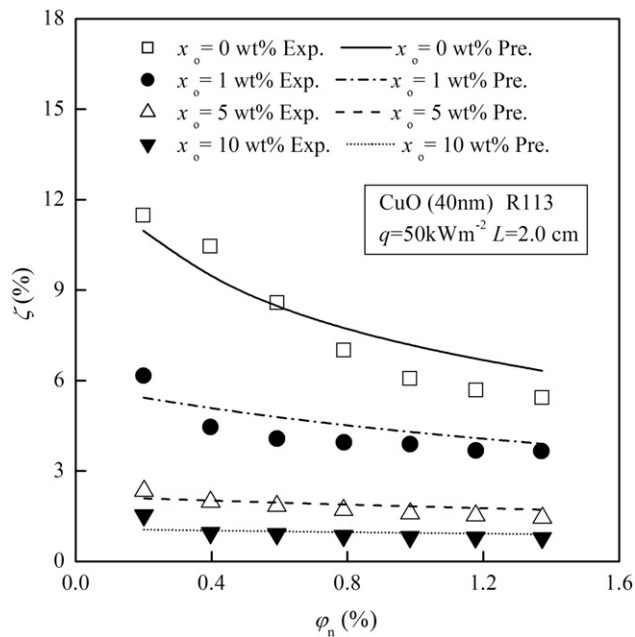
with 96% of the experimental data within a deviation of ±20%, and the mean deviation is 12.9%.

Fig. 8 shows the comparison between the predicted values of the model with the experimental data for different heat fluxes. It can be seen that both the migration ratio of nanoparticles predicted by the model and the experimental data decrease with the increase of heat flux. This phenomenon is resulted from the effect of heat flux on the velocity of departure bubble, and this effect can be predicted by the bubble departure sub-model. It can also be seen that the predicted

Fig. 7 — Comparison between the predicted values of the model with the experimental data for different mass fractions of lubricating oil.

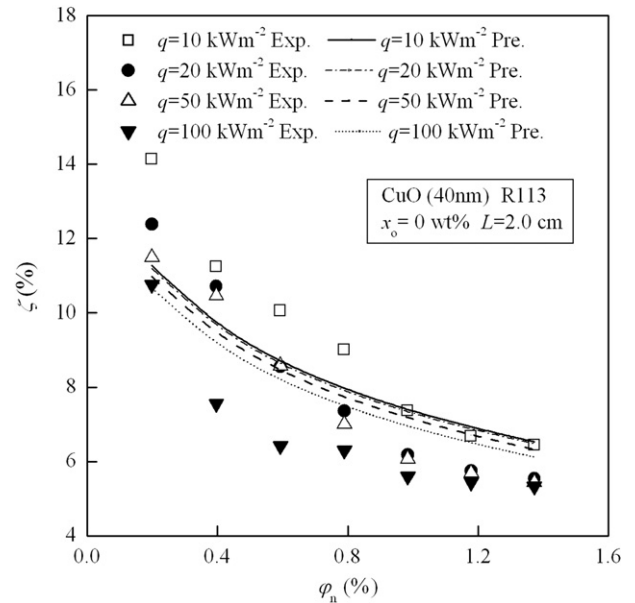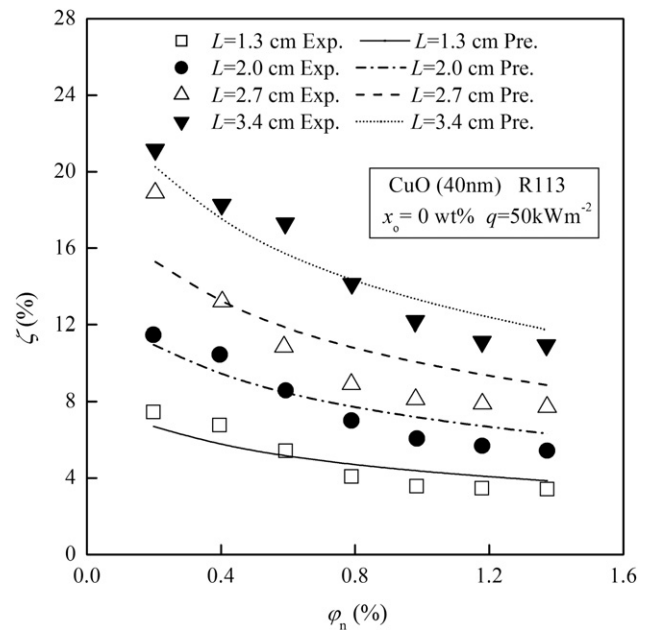Fig. 9 — Comparison between the predicted values of the model with the experimental data for different initial liquid-level heights.

values of the model can agree with 86% of the experimental data within a deviation of $\pm 20\%$, and the mean deviation is 12.6%.

Fig. 9 shows the comparison between the predicted values of the model with the experimental data for different initial liquid-level heights. It can be seen that both the migration ratio of nanoparticles predicted by the model and the experimental data increase with the increase of initial liquid-level height. This phenomenon is resulted from the effects of initial liquid-level height on the nanoparticles escape probability as well as the bubble rising time duration, and these effects can be predicted by the nanoparticles escape sub-model as well as the migration ratio sub-model. It can also be seen that the predicted values of the model can agree with 89% of the experimental data within a deviation of $\pm 20\%$, and the mean deviation is 12%.

In the present model, four sub-models including the bubble departure sub-model, the bubble and nanoparticle kinetics sub-model, the nanoparticles−bubble interaction sub-model and the nanoparticles escape sub-model are built to describe the whole physical process of the nanoparticles migration. In these sub-models, some parameters (i.e., the departure diameter of bubble, the departure frequency of bubble, the resistance coefficient on the bubble, the Brownian force on the nanoparticle and the nanoparticles capture efficiency) need to be calculated by the empirical correlations. Cole−Rohsenow correlation, Malenkov correlation, Tomiyama et al. correlation, Li and Ahmadi correlation and Edzwald correlation are used in the present model to calculate the above parameters respectively. As these existing empirical correlations have good accuracy, the reliability of the present model can be guaranteed.

In summary, the predicted values of the model agree with 90% of the existing experimental data of migration ratio of nanoparticles within a deviation of $\pm 20\%$, and the mean deviation is 12.1%. The model can predict the influences of nanoparticle type, nanoparticle size, refrigerant type, mass fraction of lubricating oil, heat flux and initial liquid-level height on the migration of nanoparticles.

5. Conclusions

The migration of nanoparticles from liquid-phase to vapor-phase in the refrigerant-based nanofluid pool boiling can be divided to four processes including the departure of bubble from the heating surface, the movement of bubble and nanoparticles in the liquid-phase, the capture of nano-particles by bubble, and the escape of nanoparticles from the liquid−vapor interface. Using dynamic model and introducing some parameters such as the nanoparticles capture efficiency and the nanoparticles escape probability are effective to predict the migration ratio of nanoparticles.

The model proposed in this study can predict the influences of nanoparticle type, nanoparticle size, refrigerant type, mass fraction of lubricating oil, heat flux and initial liquid-level height on the migration of nanoparticles. The migration ratio of nanoparticles predicted by the model can agree with 90% of the experimental data of within a deviation of $\pm 20\%$, and the mean deviation is 12.1%.

Appendix I. Calculation of the properties of liquid-phase with nanoparticles.

Property	Model for calculating property	Author
Specific heat (J kg^{-1} K^{-1})	$C_{p,L,n} = (1 - \varphi_n)C_{p,L} + \varphi_n C_{p,n}$ (A1) $C_{p,L} = (1 - x_o)C_{p,r} + x_o C_{p,o}$ (A2)	Pak and Cho (1998) Jensen and Jackman (1984)
Viscosity (Pa s)	$\mu_{L,n} = \mu_L \dfrac{1}{(1 - \varphi_n)^{2.5}}$ (A3) $\mu_L = e^{(x_o \ln \mu_o + (1 - x_o) \ln \mu_r)}$ (A4)	Brinkman (1952) Kedzierski et al. (1993)
Surface tension (N m^{-1})	$\sigma_{L,n} = \sigma_L$ (A5) $\sigma_L = \sigma_r + (\sigma_o - \sigma_r)x_o^{0.5}$ (A6)	Das et al. (2003) Jensen and Jackman (1984)
Density (kg m^{-3})	$\rho_{L,n} = (1 - \varphi_n)\rho_L + \varphi_n \rho_n$ (A7) $\rho_L = \left(\dfrac{x_o}{\rho_o} + \dfrac{1 - x_o}{\rho_r}\right)^{-1}$ (A8)	
Volume fraction of nanoparticles in the liquid-phase with nanoparticles (vol%)	$\varphi_n = \dfrac{m_{n,t}\rho_r}{m_{n,t}\rho_r + (m_o + m_{r0} - \frac{\pi}{6}\rho_{b0}d_{b0}^3 NfAt)\rho_n}$ (A9)	
Mass fraction of lubricating oil in the liquid refrigerant-oil mixture (wt%)	$x_o = \dfrac{m_o}{m_o + m_{r0} - \frac{\pi}{6}\rho_{b0}d_{b0}^3 NfAt}$ (A10)	

Appendix II. Equations used in the simulation.

Sub-model	Equation	Function
Bubble departure sub-model	$d_{b0} = 4.65 \times 10^{-4}$ $\left(\dfrac{\rho_{L,n} C_{p,L,n} T_{sat}}{\rho_{b0} h_{fg}}\right)^{\frac{5}{4}} \left(\dfrac{\sigma_{L,n}}{g(\rho_{L,n} - \rho_{b0})}\right)^{\frac{1}{2}}$ (A11)	Calculate the departure diameter of bubble
	$f = \dfrac{1}{\pi d_{b0}}\left\{\left[\dfrac{d_{b0} g(\rho_{L,n} - \rho_{b0})}{2(\rho_{L,n} + \rho_{b0})} + \dfrac{2\sigma_{L,n}(\rho_{L,n} - \rho_{b0})g}{d_{b0} g(\rho_{L,n} + \rho_{b0})}\right]^{1/2} + \dfrac{q}{h_{fg}\rho_{b0}}\right\}$ (A12)	Calculate the departure frequency of bubble
	$v_{b0} = \left[\dfrac{d_{b0} g(\rho_{L,n} - \rho_{b0})}{2(\rho_{L,n} + \rho_{b0})} + \dfrac{2\sigma_{L,n}(\rho_{L,n} - \rho_{b0})g}{d_{b0} g(\rho_{L,n} + \rho_{b0})}\right]^{1/2} + \dfrac{q}{h_{fg}\rho_{b0}}$ (A13)	Calculate the velocity of departure bubble
	$N = \dfrac{q}{h_{fg}\rho_{b0}\dfrac{\pi}{6}d_{b0}^3 f}$ (A14)	Calculate the active nucleation sites density
Bubble and nanoparticle kinetics sub-model	$\overrightarrow{F}_{total,b} = \overrightarrow{F}_{re,b} + \overrightarrow{F}_{buo,b} + \overrightarrow{F}_{g,b}$ (A15)	Calculate the forces on the bubble
	$F_{buo,b} = \dfrac{\pi}{6}d_b^3 \rho_{L,n} g$ (A16)	
	$F_{g,b} = \dfrac{\pi}{6}d_{b0}^3 \rho_{b0} g$ (A17)	
	$F_{re,b} = \dfrac{\pi}{8}d_b^2 \rho_{L,n} C_D v_b^2$ (A18-a)	
	$C_D = \max\left[\dfrac{24}{Re}(1 + 0.15 Re^{0.687}), \dfrac{8}{3}\dfrac{Eo}{Eo+4}\right]$ (A18-b)	
	$v_{b,t} = v_{b,t-\Delta t} + \int_0^{\Delta t} F_{total,b}\left/\left(\dfrac{\pi}{6}d_{b0}^3 \rho_{b0}\right)\right. dt$ (A19)	Calculate the velocity of rising bubble
	$Loc_{b,t} = Loc_{b,t-\Delta t} + \int_0^{\Delta t} v_b(t) dt$ (A20)	Calculate the location of rising bubble
	$L_t = \dfrac{m_{L0} - NfA\left(\dfrac{\pi}{6}\rho_{b0}d_{b0}^3\right)t}{\rho_L A}$ (A21)	Calculate the liquid-level height
	$\dfrac{d_{b0}^3 \rho_{b0} R_m T_{sat}}{M d_{b,t}^3} - \dfrac{4\sigma_{L,n}}{d_{b,t}} = \dfrac{\rho_{L,n} g}{\rho_L A}\left(m_{L0} - \dfrac{\pi}{6}NfA\rho_{b0}d_{b0}^3 t - \rho_L A Loc_{b,t}\right) + P_{am}$ (A22)	Calculate the diameter of bubble
	$\overrightarrow{F}_{total,n} = \overrightarrow{F}_{re,n} + \overrightarrow{F}_{buo,n} + \overrightarrow{F}_{g,n} + \overrightarrow{F}_{Brown,n}$ (A23)	Calculate the forces on the nanoparticle
	$F_{buo,n} = \dfrac{\pi}{6}d_n^3 \rho_L g$ (A24)	
	$F_{g,n} = \dfrac{\pi}{6}d_n^3 \rho_n g$ (A25)	
	$F_{re,n} = 3\pi \mu_L d_n v_n$ (A26)	
	$F_{Brown,n} = G\sqrt{\dfrac{216\mu_L k_B T_{sat}}{\pi d_n^5 \rho_n \Delta t}}$ (A27)	
	$v_{n,t} = v_{n,t-\Delta t} + \int_0^{\Delta t} F_{total,n}\left/\left(\dfrac{\pi}{6}d_n^3 \rho_n\right)\right. dt$ (A28)	Calculate the velocity of nanoparticle
Nanoparticles-bubble interaction sub-model	$E_t = 0.9\left(\dfrac{k_B T_{sat}}{\mu_{L,n}d_{b,t}d_n v_{b,t}}\right)^{\frac{2}{3}}$ (A29)	Calculate the nanoparticles capture efficiency
Nanoparticles escape sub-model	$P(D_i) = \dfrac{\arctan\left(\dfrac{D_i}{H - L_t}\right) + \arctan\left(\dfrac{D - D_i}{H - L_t}\right)}{2\pi}$ (A30)	Calculate the nanoparticles escape probability

Appendix (*continued*)		
Sub-model	Equation	Function
Migration ratio sub-model	$-\frac{m_{n,t+\Delta t}-m_{n,t}}{\Delta t} = \frac{\pi}{4}(d_{b,t}+d_n)^2$ $(v_{b,t}+v_{n,t})C_t n_b(\Delta t)E_t$ (A31)	Calculate the mass of nanoparticles in the liquid-phase
	$C_t = \dfrac{m_{n,t}\rho_L}{m_{L,0}-NfA\left(\frac{\pi}{6}\rho_{b0}d_{b0}^3\right)t}$ (A32) $n_b(\Delta t)=NfA\Delta t$ (A33)	
	$\xi_{t_0-t_j}=\dfrac{1}{m_{n0}}\displaystyle\sum_{i=0}^{j-1}\Delta m_{n,t_i-t_{i+1}}P_{t_{i+1}}$ (A34)	Calculate the migration ratio of nanoparticles

REFERENCES

Brinkman, H.C., 1952. The viscosity of concentrated suspensions and solution. J. Chem. Phys. 20, 571–581.

Buongiorno, J., 2006. Convective transport in nanofluids. J. Heat Transfer 128, 240–250.

Cole, R., Rosenhow, W., 1969. Correlation of bubble departure diameters for boiling of saturated liquids. Chem. Eng. Prog. Symp. Ser. 65 (92), 211–213.

Dai, Z.F., Fornasiero, D., Ralston, J., 1999. Particle-bubble attachment in mineral flotation. J. Colloid Interface Sci. 217, 70–76.

Das, S.K., Putra, N., Roetzel, W., 2003. Pool boiling characteristics of nano-fluids. Int. J. Heat Mass Transfer 46 (5), 851–862.

Ding, G.L., Peng, H., Jiang, W.T., Gao, Y.F., 2009. The migration characteristics of nanoparticles in the pool boiling process of nanorefrigerant and nanorefrigerant-oil mixture. Int. J. Refrigeration 32 (1), 114–123.

Ding, Y.L., Wen, D.S., 2005. Particle migration in a flow of nanoparticle suspensions. Powder Technol. 149, 84–92.

Edzwald, J.K., Malley, J.P., Yu, C., 1990. A conceptual model for dissolved air flotation in water treatment. Water Supply 8, 141–150.

Fung, M.S., Hamdullahpr, F., 1993. A gas and particle flow model in the freeboard of a fluidized bed based on bubble coalescence. Powder Technol. 74, 121–133.

Hu, H.T., Ding, G.L., Wang, K.J., 2008. Heat transfer characteristics of R410A-oil mixture flow boiling inside a 7 mm straight microfin tube. Int. J. Refrigeration 31 (6), 1081–1093.

Jensen, M.K., Jackman, D.L., 1984. Prediction of nucleate pool boiling heat transfer coefficients of refrigerant–oil mixtures. J. Heat Transfer 106, 184–190.

Kedzierski, M.A., Kaul, M.P., 1993. Horizontal nucleate flow boiling heat transfer coefficient measurements and visual observations for R12, R134a, and R134a/ester lubricant mixtures. In: Proceedings of the 6th International Symposium on Transport Phenomena in Thermal Engineering, vol. 1, p. 111–116.

Khanafer, K., Vafai, K., Lightstone, M., 2003. Buoyancy-driven heat enhancement in a two dimensional enclose utilizing nanofluids. Int. J. Heat Mass Transfer 46, 3639–3653.

Kleinstreuer, C., 2003. Two-phase Flow. Taylor & Frances, New York, pp. 133–226.

Leighton, D., Acrivos, A., 1987. The shear-induced migration of particles in concentrated suspensions. J. Fluid Mech. 181, 415–439.

Li, A., Ahmadi, G., 1992. Dispersion and deposition of spherical particles from point sources in a turbulent channel flow. Aerosol Sci. Technol. 16, 209–226.

Liu, S., 1999. Particle dispersion for suspension flow. Chem. Eng. Sci. 54, 873–891.

Maiga, S.E.B., Palm, S.J., Nguyen, C.T., Roy, G., Galanis, N., 2005. Heat transfer enhancement by using nanofluids in forced convection flows. Int. J. Heat Fluid Flow 26, 530–546.

Malenkov, I.G., 1971. Detachment frequency as a function of size for vapor bubbles. J. Eng. Phys. Thermophy. 20 (6), 704–708.

Morris, J.F., Brady, J.F., 1998. Pressure-driven flow of a suspension: buoyancy effects. Int. J. Multiphase Flow 24, 105–130.

Namburu, P.K., Das, D.K., Tanguturi, K.M., Vajjha, R.S., 2009. Numerical study of turbulent flow and heat transfer characteristics of nanofluids considering variable properties. Int. J. Thermal Sci. 48, 290–302.

Nguyen, A.V., George, P., Jameson, G.J., 2006. Demonstration of a minimum in the recovery of nanoparticles by flotation: theory and experiment. Chem. Eng. Sci. 61, 2494–2509.

Nguyen, A.V., Ralston, J., Schulze, H.J., 1998. On modelling of bubble–particle attachment probability in flotation. Int. J. Miner. Process. 53, 225–249.

Pak, B.C., Cho, Y.I., 1998. Hydrodynamic and heat transfer study of dispersed fluids with submicron metallic oxide particles. Exp. Heat Transfer 11 (2), 151–170.

Peng, H., Ding, G.L., Hu, H.T., 2011. Influences of refrigerant-based nanofluid composition and heating condition on the migration of nanoparticles during pool boiling. Part I: experimental measurement. Int. J. Refrigeration 34 (8), 1823–1832.

Phillips, R.J., Armstrong, R.C., Brown, R.A., Graham, A.L., Abbott, J. R., 1992. A constitutive equation for concentrated suspensions that accounts for shear-induced particle migration. Phys. Fluids A 4, 30–40.

Putra, N., Roetzel, W., Das, S., 2003. Natural convection of nano-fluids. Heat Mass Transfer 39 (8–9), 775–784.

Ralston, J., Dukhin, S.S., 1999. The interaction between particles and bubbles. Colloids Surfaces A: Physicochem. Eng. Aspects 151, 3–14.

Tomiyama, A., Kataoka, I., Zun, I., Sakaguchi, T., 1998. Drag coefficients of single bubble under normal and micro gravity conditions. JSME 41 (2), 472–479.

Wen, D.S., Ding, Y.L., 2005. Formulation of nanofluids for natural convective heat transfer applications. Int. J. Heat Fluid Flow 26 (6), 855–864.

Wen, D.S., Zhang, L., He, Y.R., 2009. Flow and migration of nanoparticle in a single channel. Heat Mass Transfer 45, 1061–1067.

Xuan, Y.M., Yao, Z.P., 2005. Lattice Boltzmann model for nanofluids. Heat Mass Transfer 41, 199–205.

Yoon, R.H., 2000. The role of hydrodynamic and surface forces in bubble–particle interaction. Int. J. Miner. Process. 58, 129–143.